SAND2014-20214C

Complex Geometry Effects on Subsonic Cavity Flows

Katya M. Casper*, Justin L. Wagner†, Steven J. Beresh‡, John F. Henfling§,
Russell W. Spillers,¶ and Brian O. M. Pruett‖
Sandia National Laboratories, Albuquerque, NM 87185

The flow over aircraft bays are often represented using rectangular cavities; however, this simplification neglects many features of the actual flight geometry which could affect the resonant pressure field and resulting loading in the bay. To address this shortcoming, a complex cavity geometry was developed to incorporate more realistic aircraft-bay features including shaped inlets, internal cavity variations, and doors. A parametric study of these features was conducted at Mach 0.8. Much higher frequency content and higher-amplitude fluctuations were found with the presence of the complex geometry that could produce severe loading conditions for stores carried within the bays. High-frequency resonances were generated by features that constricted the flow such as leading edge overhangs, internal cavity variations, and the presence of closed doors. Also, the Rossiter modes of the complex configurations were usually shifted in frequency from the simple rectangular cavity, and many modes had much higher amplitudes. Broadband frequency components measured at the aft wall of the complex cavities were also significantly higher than in the rectangular geometry. These changes highlight the need to consider complex geometric effects when predicting the flight loading of aircraft bays.

Nomenclature

D	cavity depth (mm)	Re	freestream unit Reynolds number (1/m)
f	frequency (kHz)	St	Strouhal number, fL/U_∞
L	cavity length (mm)	U_∞	freestream velocity (m/s)
M	freestream Mach number	W	cavity width (mm)
P_0	total pressure (kPa)		
q_∞	freestream dynamic pressure (kPa)		

I. Introduction

The flow over aircraft bays can generate significant structural loading caused by resonant pressure fluctuations created in the bay. This resonance is typical of cavity flows, which have been extensively studied over the years.[1,2] The flow over a cavity can set up a feedback loop between the free shear layer and the cavity's acoustic field that creates resonant tones or 'Rossiter' modes in the cavity.[3] This typically occurs in 'open' subsonic cavity flows when the cavity length-to-depth ratio L/D is less than about 6-8.[4] The amplitude of the modes can be quite large, and sound pressure levels (SPL) greater than 170 dB have been reported.[5] The frequencies of these modes in compressible flow can be estimated using Heller and Bliss's semi-empirical

*Senior Member of the Technical Staff, Engineering Sciences Center, Member AIAA, kmcaspe@sandia.gov, (505) 844-1574
†Senior Member of the Technical Staff, Engineering Sciences Center, Member AIAA
‡Distinguished Member of the Technical Staff, Engineering Sciences Center, Associate Fellow AIAA
§Distinguished Technologist, Member AIAA
¶Principal Technologist
‖Senior Technologist

Sandia National Laboratories is a multi-program laboratory managed and operated by Sandia Corporation, a wholly owned subsidiary of Lockheed Martin Corporation, for the U.S. Department of Energy's National Nuclear Security Administration under contract DE-AC04-94AL85000.

method.[6] However, the distribution of the mode amplitudes and their frequencies varies greatly depending on flow condition and cavity geometry.

Previous experiments in rectangular cavities of various width and depth have been conducted to study the unsteady fluctuations and their coupling to store vibration.[7] Velocimetry measurements of a rectangular cavity in supersonic flow have shown that the cavity width alters the flow field structure.[8] However, there are limitations when applying this work to actual aircraft bays, which have many complex features that are not captured by a simple rectangular cavity geometry.[9] For example, the flow approaching the cavity leading edge is not necessarily uniform. The presence of the fuselage on the aircraft is an important difference between flight and almost every wind-tunnel test on a rectangular cavity. Also, the cavity is not necessarily aligned with the incoming flow. Previous studies have shown that both cavities in yaw[10–12] or swept cavities[13] can exhibit different mode amplitude distributions or even mode frequencies in some cases.

Also, at the upstream lip of some aircraft bays, the shape of the fuselage and cut of the inlet creates a geometry that sets up a differential flow expansion. This generates strong streamwise vorticity that entrains high-speed fluid into the bay and can also affect the shear layer structure.[9] The upstream lip of the bay can also be higher above the cavity floor than the downstream edge which changes where the shear layer impinges on the back wall of the cavity. This impingement plays a role in the feedback loop governing the cavity dynamics.[3,14–17] Also, the doors of the aircraft bay alter the cavity dynamics.[9,18–20] For example, open doors can modify the side spillage into the bay or closed doors can act like a lid and affect the cavity resonance. Finally, the internal geometry plays a role in the unsteady dynamics because the width or depth of the cavity varies within the bay. For example, several studies have shown that the presence of a store in the cavity, which alters the cavity volume, can change the cavity resonance.[5,7,18,21–23] All of these geometric features may change the acoustic environment within the cavity and thus the vibrational excitation of stores contained within.

Limited work has been done to explore these configurational differences[9,13,15,18,24] and much of this work has focused on the control of pressure fluctuations in these complex geometries, not on understanding the differences from simple geometries. To address this shortcoming, a complex cavity geometry was designed to allow features representing a realistic aircraft-bay geometry to be incorporated one by one. A parametric study of these geometric features was conducted in the Sandia Trisonic Wind Tunnel (TWT) at Mach 0.8 to isolate important parameters for the pressure loading in aircraft bays and to investigate the limits of rectangular cavities in representing flight geometry. These results are compared to supersonic measurements reported in Ref. 25.

II. Experimental Setup

II.A. Sandia Trisonic Wind Tunnel

Experiments are performed in Sandia's Trisonic Wind Tunnel. This is a blowdown-to-atmosphere facility using air as the test gas. The full test section is 305×305 mm and is enclosed in a pressurized plenum. Fig. 1 shows the cavity installed on the top wall of the test section for subsonic tests. Recent work has identified an optimal wall configuration with acoustic dampening to reduce tunnel mode interference with the cavity flows.[26] This interference is due to a resonance coupling with the radiated acoustic field from the cavity. The present results use the optimal configuration identified in the study; a porous floor insert and one porous sidewall helps ensure that tunnel modes are dramatically reduced from a solid wall configuration.

Typical run conditions are given in Table 1. The Mach number is computed from a centerline static pressure measurement 21.9 cm upstream of the cavity leading edge. The incoming boundary layer to the cavity is fully turbulent. Previous (unpublished) measurements have shown that the boundary layer thickness at the cavity leading edge is about 0.3–0.4 D. The stagnation temperature is held constant at $321 \pm 2K$. The walls of the test section remain near room temperature at $307 \pm 3K$.

Table 1. Typical run conditions.

M_∞	q_∞ (kPa)	P_0 (kPa)	$Re \times 10^6/m$
0.8	33	112	13

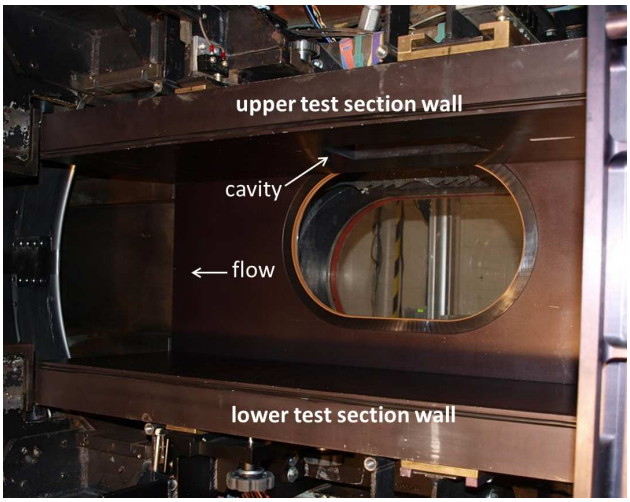

Figure 1. Complex cavity installed in the TWT subsonic full nozzle.

II.B. Cavity design and apparatus

The complex cavity apparatus is built up from a simple rectangular cutout that is integrated into a tunnel wall insert (Fig. 2). This cavity has a length, width, and depth of 203, 102, and 29 mm, respectively. The L/D ratio of 7 categorizes this simple cavity flow at the upper limit of 'open' in subsonic flows.[4] To create distinct complex geometric configurations, different pieces can be added to the front and sides of the rectangular cavity. The basic sensor layout and coordinate system remains the same in the complex geometry. Table 2 lists the various configurations that can be created.

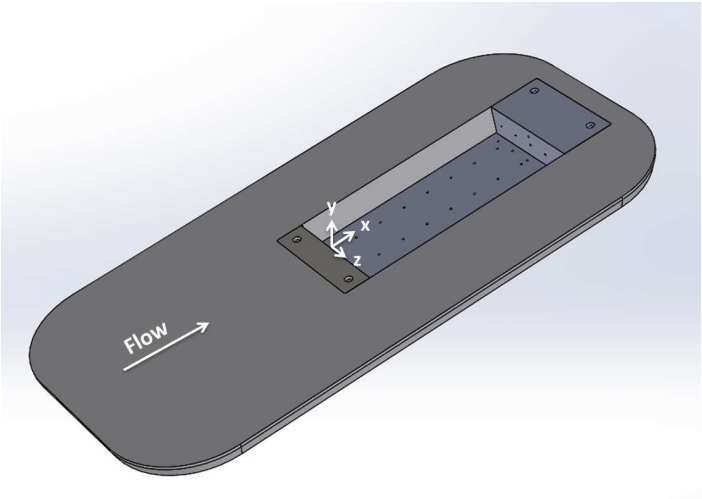

Figure 2. Simple rectangular cavity tunnel insert.

The non-uniform inlet flow found in flight is simulated in the complex geometry with different ramps at the leading edge of the cavity. A smooth 5.7° ramp is the baseline case for comparison (Fig. 3(a)). Two side ramps are also added to this configuration to transition from the higher leading edge to the flat plate geometry on the sides of the cavity. The front ramp lifts the leading edge of the cavity 12.7 mm above the trailing edge and effectively changes the L/D of the cavity along its length from 5 at the leading edge to 7 at the trailing edge. Although these ramps have planar surfaces rather than curved surfaces like a real aircraft, the difference is expected to have little effect on the results since the ramp angles are below limits for incipient separation in both subsonic and supersonic flow.[27,28]

The next inlet configuration has a ramp with a centered cutout or scoop (Fig. 3(b)). The scoop addresses the effect the engine inlet has on the incoming flow to the cavity. Some of the flow bypasses the inlets and

passes through a narrow channel leading up to the bay. This nonuniform flow then passes over a jagged leading edge with a sawtooth pattern that overhangs the front portion of the bay. A similar tooth can be added to the complex geometry to simulate this configuration (Fig. 3(c)). Additional complex geometry configurations were made with offset cutout and sawtooth designs that exaggerate the asymmetries in the flow and move the resulting streamwise-aligned vortex away from the centerline of the cavity (Figs. 3(d) and 3(e)).

The internal geometry of the cavity can also be varied. In many flight hardware, there is a section at the rear of the aircraft bay containing ductwork. This section effectively decreases the width of the cavity, which will influence the cavity dynamics. An internal insert was designed to simulate this effect (Fig. 4(a)). This insert is 101.6 mm long and 19.1 mm wide, which changes the L/W from 2 to 2.5 over the downstream half of the cavity. A ramped floor was also designed which more closely represents the flight geometry. The ramp changes the L/D ratio of the cavity from 12 at the leading edge of the cavity to 7 at the trailing edge, which will affect the cavity dynamics and resulting pressure fluctuations. This ramped floor can be tested in conjunction with all the configurations in Table 2.

Another important parameter is the presence of the aircraft-bay doors. The complex geometry can be tested without doors or both doors can be installed open (or closed) or with one or the other door open (Figs. 4(b)–4(c)). The doors are not the same because of the asymmetric sawtooth at the leading edge.

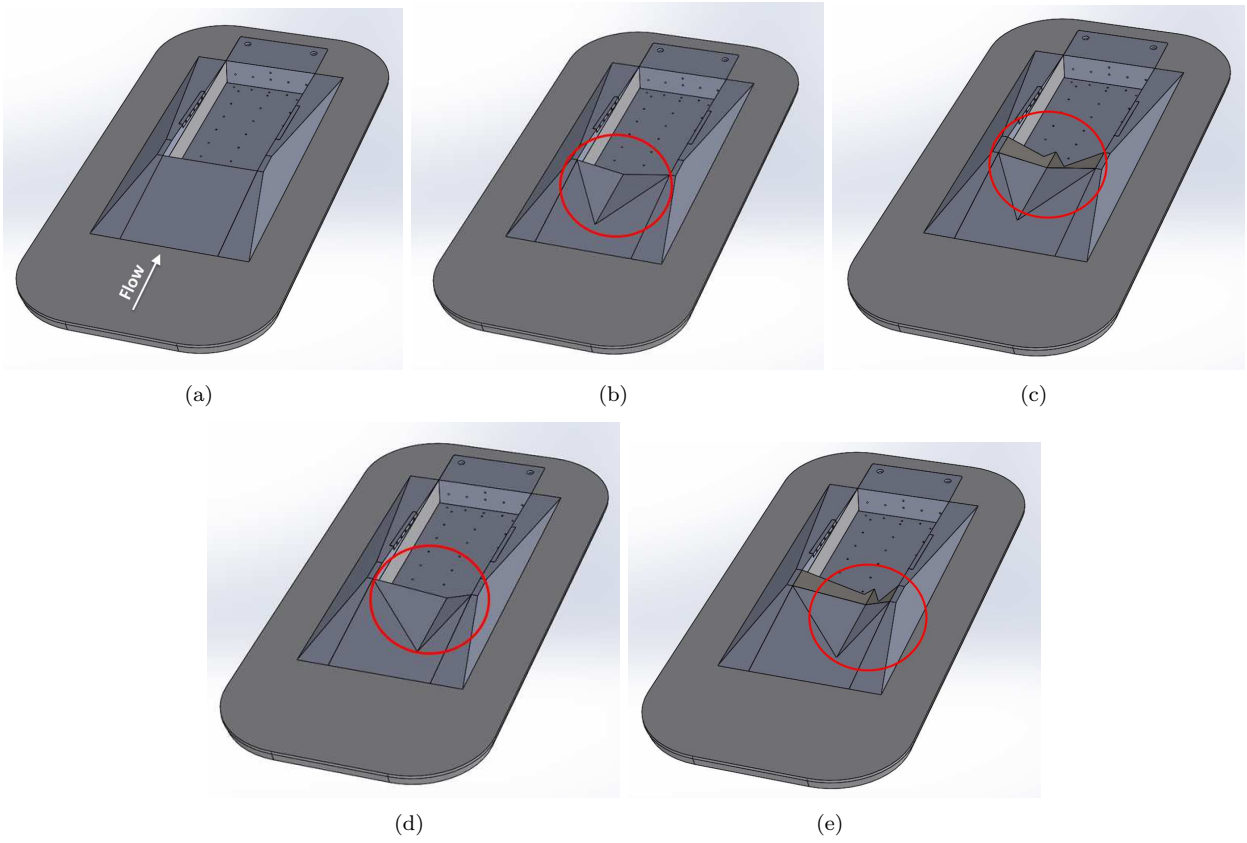

Figure 3. Complex geometry leading edge configurations (a) Baseline cavity (smooth ramp); (b) Center scoop (c) Center scoop and tooth; (d) Offset scoop; (e) Offset scoop and tooth.

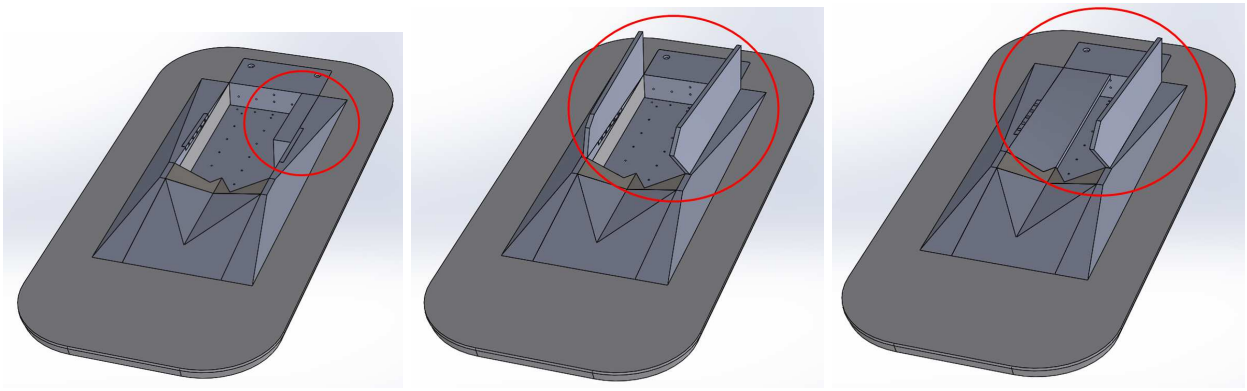

(a) (b) (c)

Figure 4. Additional complex geometry configurations (a) Side insert which changes the width of the cavity along its length; (b) Two doors open; (c) One door open and one door closed.

II.C. Instrumentation and Data Acquisition

The complex geometry has 40 positions available for pressure measurements, 25 of which were used during testing. Five sensors are located in the spanwise direction along the forward floor of the cavity (FFP1–5, Fig. 5(a)). There is also a line of sensors down the center of the cavity (C2-C7). Two sensors are located on either side of sensor C4 in the spanwise direction and are designated L4 and R4. There is another spanwise line of sensors on the aft wall of the cavity (AWP1–5, Fig. 5(b)). A final sensor AWP6 is located on the cavity centerline, on the aft wall above sensor AWP3. A schematic of these locations with respect to the cavity geometry is shown in Fig. 5(c). When the centered tooth is installed, the front floor sensors FFP1-5 are located beneath an overhang created by the tooth. Sensor C2 is just downstream of the tooth on the cavity floor. When the side insert is installed, sensor R4 is located in front of the insert, while sensors RFP5 and AWP5 are covered.

Kulite XCQ-062-30A (or similar) pressure transducers are used to measure the unsteady cavity pressure fluctuations. These sensors have a resonant frequency of 240–300 kHz. The repeatability is approximately 0.1% of the full scale. The Kulite signal output is passed through an Endevco Model 136 DC Amplifier. This provides a 10 V excitation and is also used to supply a gain of 50–100. A Krohn-Hite Model 3384 Tunable Active Filter is used to provide a 50 kHz anti-aliasing low-pass Bessel filter. This filter has eight poles and provides 48 dB attenuation per octave. The Kulite sampling frequency is typically 500 kHz. Data are acquired using a National Instruments PXI-1042 chassis with 14-bit PXI-6133 modules (10 MHz bandwidth).

Table 2. Complex geometry configurations, each configuration can be tested with either a flat or ramped floor.

	Configuration	Side Ramps	Front Ramp	Tooth	L Door	R Door	Side Insert
1	Simple rectangular cavity	No	No	No	No	No	No
2	Baseline cavity	Yes	Smooth	No	No	No	No
3	Baseline cavity with side insert	Yes	Smooth	No	No	No	Yes
4	Baseline cavity with center scoop	Yes	Center scoop	No	No	No	No
5	Baseline cavity with center scoop and tooth	Yes	Center scoop	Center	No	No	No
6	Baseline cavity with center scoop and tooth and side insert	Yes	Center scoop	Center	No	No	Yes
7	Baseline cavity with offset scoop	Yes	Offset scoop	No	No	No	No
8	Baseline cavity with offset scoop and tooth	Yes	Offset scoop	Offset	No	No	No
9	Baseline cavity with offset scoop and tooth and side insert	Yes	Offset scoop	Offset	No	No	Yes
10	Baseline cavity with center scoop and tooth and open doors	Yes	Center scoop	Center	Open	Open	No
11	Baseline cavity with center scoop and tooth, open doors and side insert	Yes	Center scoop	Center	Open	Open	Yes
12	Baseline cavity with center scoop and tooth, L door open and R door closed	Yes	Center scoop	Center	Open	Closed	No
13	Baseline cavity with center scoop and tooth, R door open, L door closed	Yes	Center scoop	Center	Closed	Open	No
14	Baseline cavity with center scoop and tooth, R door open, L door closed and side insert	Yes	Center scoop	Center	Closed	Open	Yes
15	Baseline cavity with offset scoop and tooth and open doors	Yes	Offset scoop	Offset	Open	Open	No
16	Baseline cavity with offset scoop and tooth, open doors and side insert	Yes	Offset scoop	Offset	Open	Open	Yes
17	Baseline cavity with offset scoop and tooth, L door closed, and R door open	Yes	Offset scoop	Offset	Closed	Open	No
18	Baseline cavity with offset scoop and tooth, L door closed, R door open and side insert	Yes	Offset scoop	Offset	Closed	Open	Yes

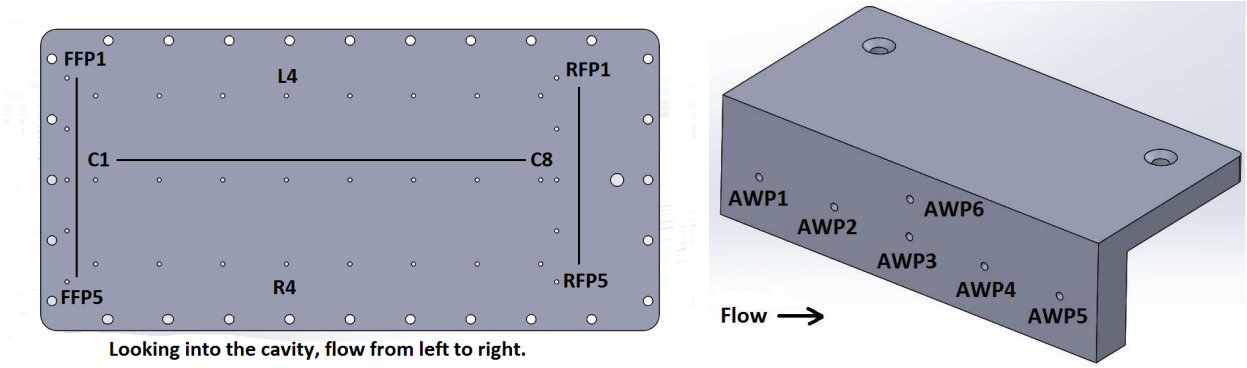

(a) (b)

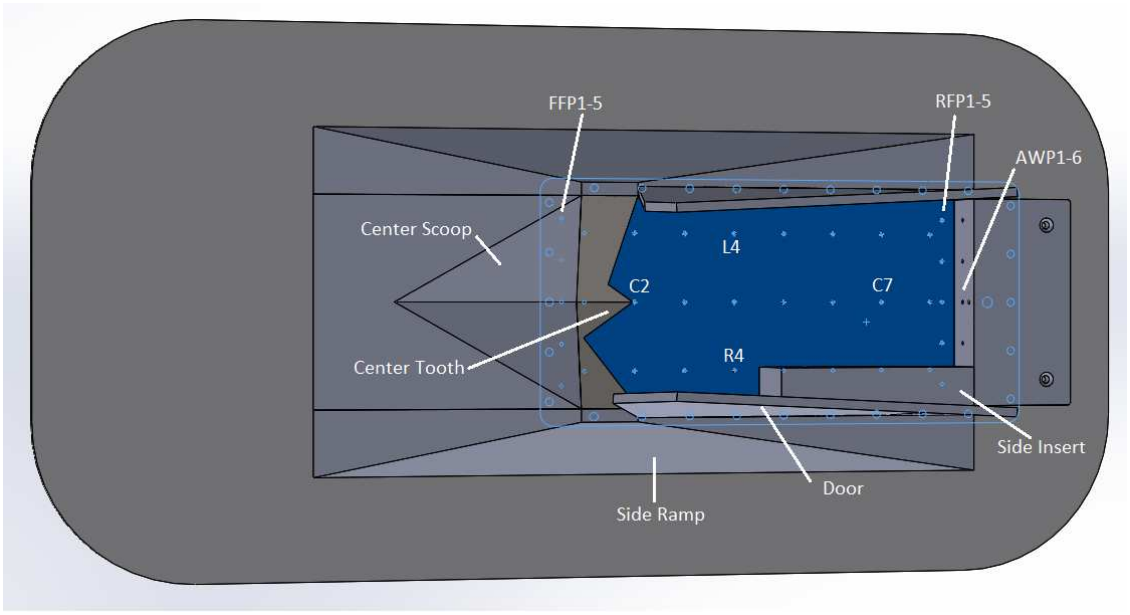

(c)

Figure 5. Complex cavity sensor locations (a) Floor plate; (b) Aft cavity wall; (c) Floor plate and aft cavity wall installed in complex geometry.

III. Experimental Results

III.A. Simple rectangular cavity

The starting point for all complex configurations is the simple rectangular cavity. Fig. 6 shows the power spectral density of pressure fluctuations in the rectangular cavity at Mach 0.8. The power spectra are shown in sound pressure level (SPL) and were computed using Welch's periodogram method, Blackman windows, and 50% overlap between data segments. The frequency resolution of the spectra is 10 Hz. Resonant peaks corresponding to the Rossiter modes can be clearly seen. The frequencies of these peaks can be compared with the empirical correlation of Heller and Bliss.[6] Fig. 6(a) shows the first six predicted mode frequencies marked with dashed lines. Empirical constants of $\alpha = 0.25$ and $K = 0.57$ were used and give reasonable agreement with the data, though the predicted frequencies are higher than observed in the experiment for modes 1–3 and lower for modes 4–7.

The flow in the rectangular cavity shows good symmetry about the centerline. There are small spanwise differences in the spectra, mostly in the upstream level of broadband frequency content. However the frequency of modes remains constant across the span (Fig. 6(a)). The broadband fluctuations and modal peaks generally increase in amplitude with downstream distance (Fig. 6(b)). However, some modes seem to have nodes along the cavity floor and are not picked up at some locations. For example, mode 2 does not show up at C6 and modes 1 and 5 are absent at C4.

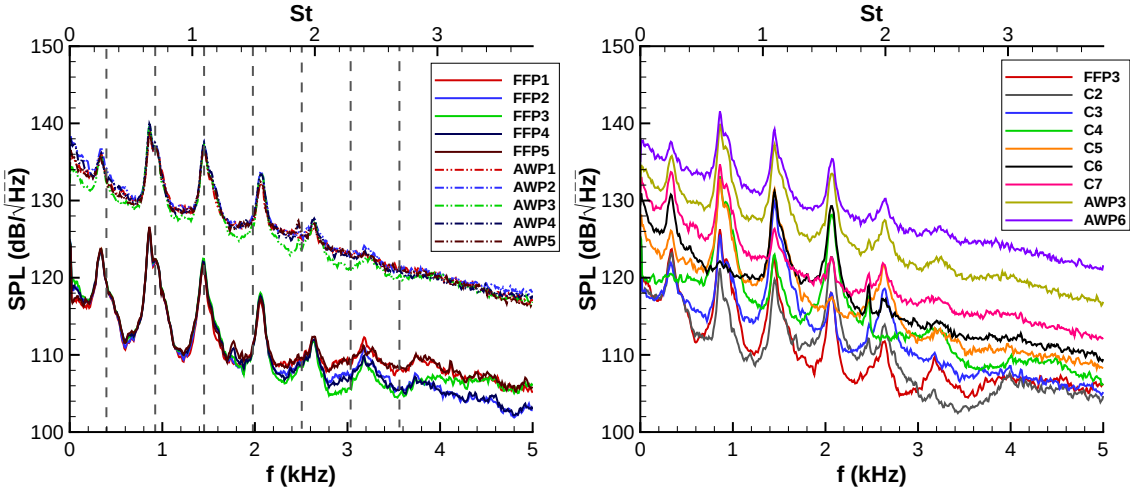

(a) (b)

Figure 6. Simple rectangular cavity measurements at Mach 0.8 (a) Front floor and aft wall sensors; (b) Centerline sensors.

III.B. Baseline cavity

Similar measurements were made with the baseline cavity configuration. As shown in Fig. 3(a), smooth front and side ramps are added to the rectangular cavity to reach this configuration. Fig. 7(a) shows a comparison of PSD's from the front centerline of the two geometries at FFP3. There are differences between the two configurations in both the mode amplitude and frequencies. In the baseline cavity, the frequency of the modes shifts up significantly between 100–300 Hz. There are also large amplitude variations when comparing the simple and baseline cavities. All mode amplitudes are lower when compared to the rectangular cavity, except for a more dominant low-frequency peak near 77 Hz at the front of the cavity. Even though the mode amplitudes vary, the broadband frequency amplitudes are similar at the front end of the cavity.

At the aft centerline of the cavity, a frequency shift of the modes is again observed. The mode amplitudes are still lower for the baseline cavity, but there are more significant differences in the level of broadband fluctuations which are much higher at the aft wall for the rectangular cavity. This large difference in both broadband fluctuations and mode amplitudes at the aft wall likely comes from the raised leading edge of the baseline configuration which lifts the shear layer higher with respect to the rear cavity wall. Previous flow control studies have shown that mode amplitudes can be reduced by this lofting, for example by using a

leading edge spoiler, which changes the feedback loop that typically creates the resonant pressure fluctuations in the cavity.[3,14–17]

To further look at the nature of the cavity flow, the cross correlation between pressure measurements at the front (FFP3) and rear (AWP3) of the cavity was computed (Fig. 7(b)). A difference can be seen between the two geometries. The simple rectangular cavity has much higher correlation levels. The cross correlation is also more periodic in nature, showing the more coherent and ordered structure of the flow in the rectangular cavity. The time lag of the dominant periodicity corresponds to the frequency of the dominant second modes observed in the PSD's for the simple rectangular cavity. On the other hand, the baseline cavity cross correlation shows very little periodicity. There is one large peak near -0.5 ms corresponding to the time it takes for acoustic disturbances in the cavity to propagate between the two sensor locations. The propagation time of the disturbances is slightly smaller than observed for the simple rectangular cavity. This difference corresponds to a frequency shift of approximately 170 Hz, consistent with the shift in frequency of the second Rossiter mode observed in the PSD's. Otherwise, there is no dominant periodicity in the cross correlation as was seen in the simple rectangular cavity. Higher frequency modes in the baseline cavity are more important to the overall pressure fluctuations, but are less correlated than in the rectangular cavity. This result is consistent with the strongest second-mode peak for the rectangular cavity PSD but weaker and more evenly distributed mode amplitudes in the baseline case.

A comparison of the coherence between fore and aft wall pressure measurements in both configurations can also be made (Fig. 8). At the front of the rectangular cavity, the coherence is near a value of one for the first four modes and then drops for the higher modes. For the baseline cavity, the coherence at the front is lower than the rectangular cavity for all modes. At the rear of the cavity, overall coherence levels are much lower for both configurations, consistent with the literature.[23,29] However, the simple rectangular cavity still has coherent peaks above 0.8 at the second and third modes. This high coherence again highlights the more resonant and ordered flow in the rectangular cavity. The baseline cavity, on the other hand, has a peak coherence of just over 0.6, which occurs for the third mode. These results are consistent with the dominant modes seen in the cross correlations and PSD's for both configurations. The difference in behavior between the two configurations is consistent with the shear layer being lofted above the aft cavity wall in the baseline cavity. This weakens the typical feedback mechanisms between the unsteady shear layer and the cavity acoustics that are dominant in the simple cavity. These changes are also consistent with results obtained in supersonic flow.[25]

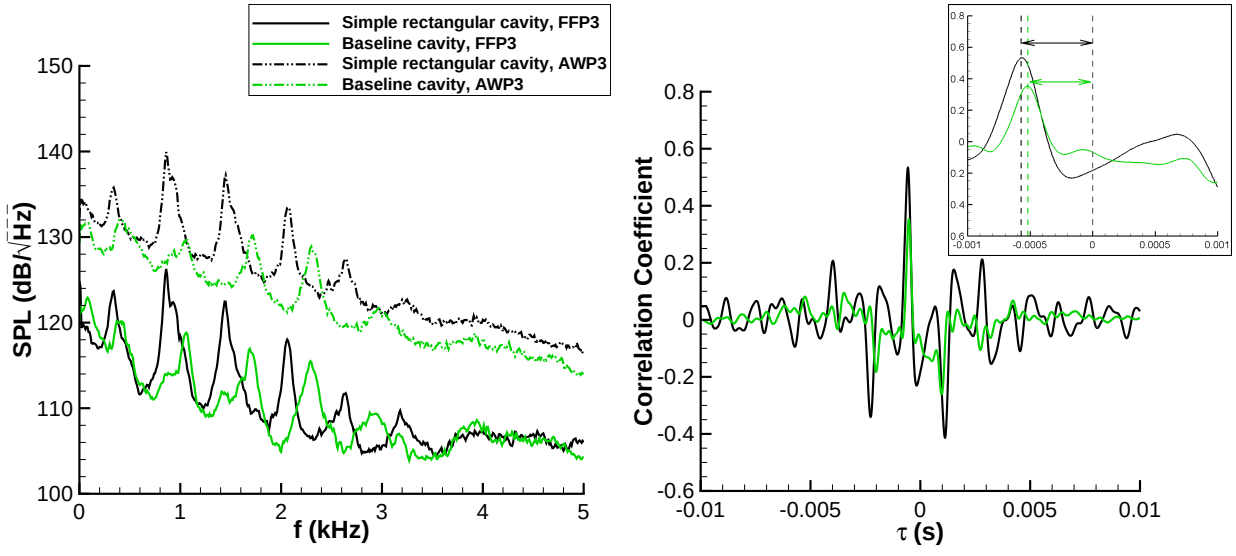

(a) (b)

Figure 7. Comparison of simple and baseline cavity at Mach 0.8 (a) Power-spectral density; (b) Fore-aft cross-correlation.

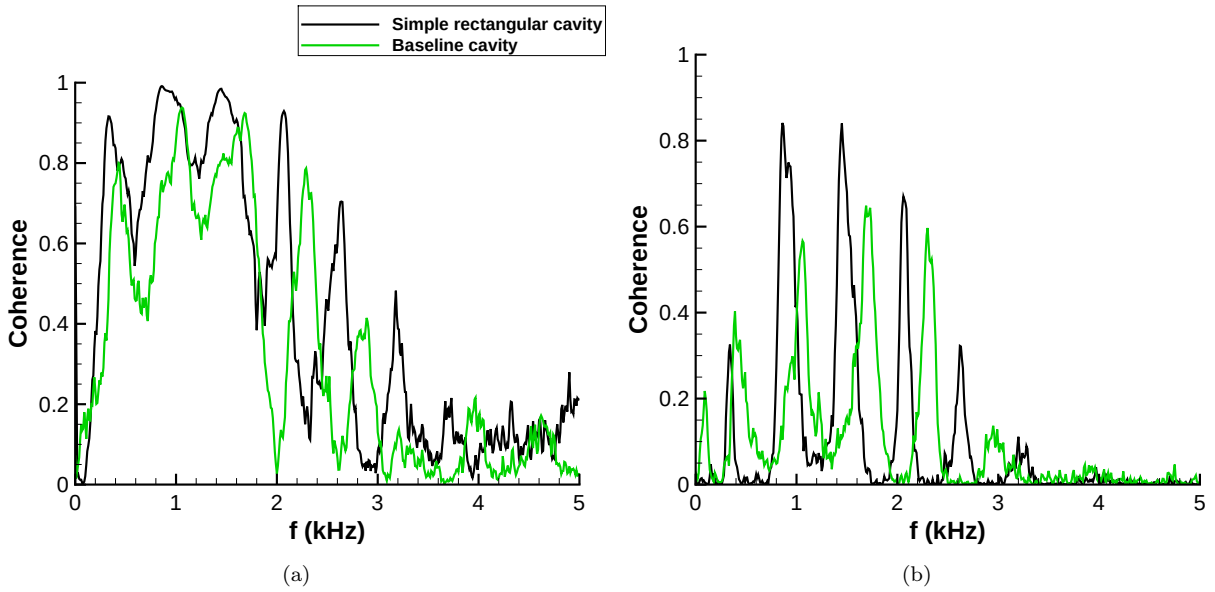

(a) (b)

Figure 8. Comparison of simple and baseline cavity coherences at Mach 0.8 (a) Front (FFP2–FFP4); (b) Aft (AWP2–AWP4).

III.C. Effect of cavity inlet flow

The effect of a non-uniform cavity inlet flow was studied by varying the inlet ramp geometry as compared to the baseline cavity configuration. Both a centered (Fig. 3(b)) and offset scoop (Fig. 3(d)) were tested. A comparison of the PSD's between the different configurations is shown in Fig. 9(a). There are no large differences between the center and offset scoops; they appear similar throughout the cavity in both the level of broadband fluctuations and the mode amplitudes.

The behavior of these two geometries is similar to the baseline cavity at FFP3. The frequency of the modes is again shifted from the rectangular cavity by 100–300 Hz. However, the mode amplitudes are higher than the baseline cavity, and there is an additional resonant peak near 3.2 kHz. This amplification occurs for all the modes, while at Mach 1.5, only the lower two modes were amplified by the presence of the scoops.[25] Further downstream, the offset and center scoop results deviate from the baseline cavity. The level of broadband fluctuations and mode amplitudes is much higher than the baseline cavity measurements. This elevated level of fluctuations at the aft wall likely come from the reduced depth of the cavity along the center of the scoop. This reduced depth is similar to that of the simple rectangular cavity and brings the shear layer back down towards the aft cavity wall. This would be expected to increase the fluctuations on the rear wall and also enhance the feedback loop feeding the mode amplitudes.[3,14–17] However, instead of approaching the rectangular cavity levels as was observed at Mach 1.5,[25] the broadband levels exceed those of the simple rectangular cavity. Even though the broadband fluctuations and mode amplitudes for both the center and offset scoops exceed those of the rectangular cavity, the cross-correlation (Fig. 9(b)) and coherence (Fig. 9(c)) levels remain lower. The spanwise non-uniformity introduced by leading edge scoop geometry likely disrupts the shear layer and its uniform impingement on the aft wall which reduces these in comparison to the rectangular cavity.

III.D. Effect of cavity leading edge configuration: asymmetric tooth

To simulate a typical flight geometry, an asymmetric tooth was added to the leading edge of the complex geometry in conjunction with the different ramp configurations (Figs. 3(c) and 3(e)). Fig. 10 shows comparisons of PSD's with and without the leading edge tooth at various locations in the cavity. An effect of the tooth is observed at the upstream end of the cavity (Figs. 10(a) – 10(b)) where much higher frequency content appear in the spectra. This enhancement is likely generated by the overhang the tooth creates at the front of the cavity. This overhang constricts the flow and leads to additional resonances in that location. This effect is particularly evident at FFP1 (Fig. 10(a)) where a large peak near 8.25 kHz is seen in the PSD. This frequency is close to the estimated closed box tone for stagnant flow corresponding to the height of the

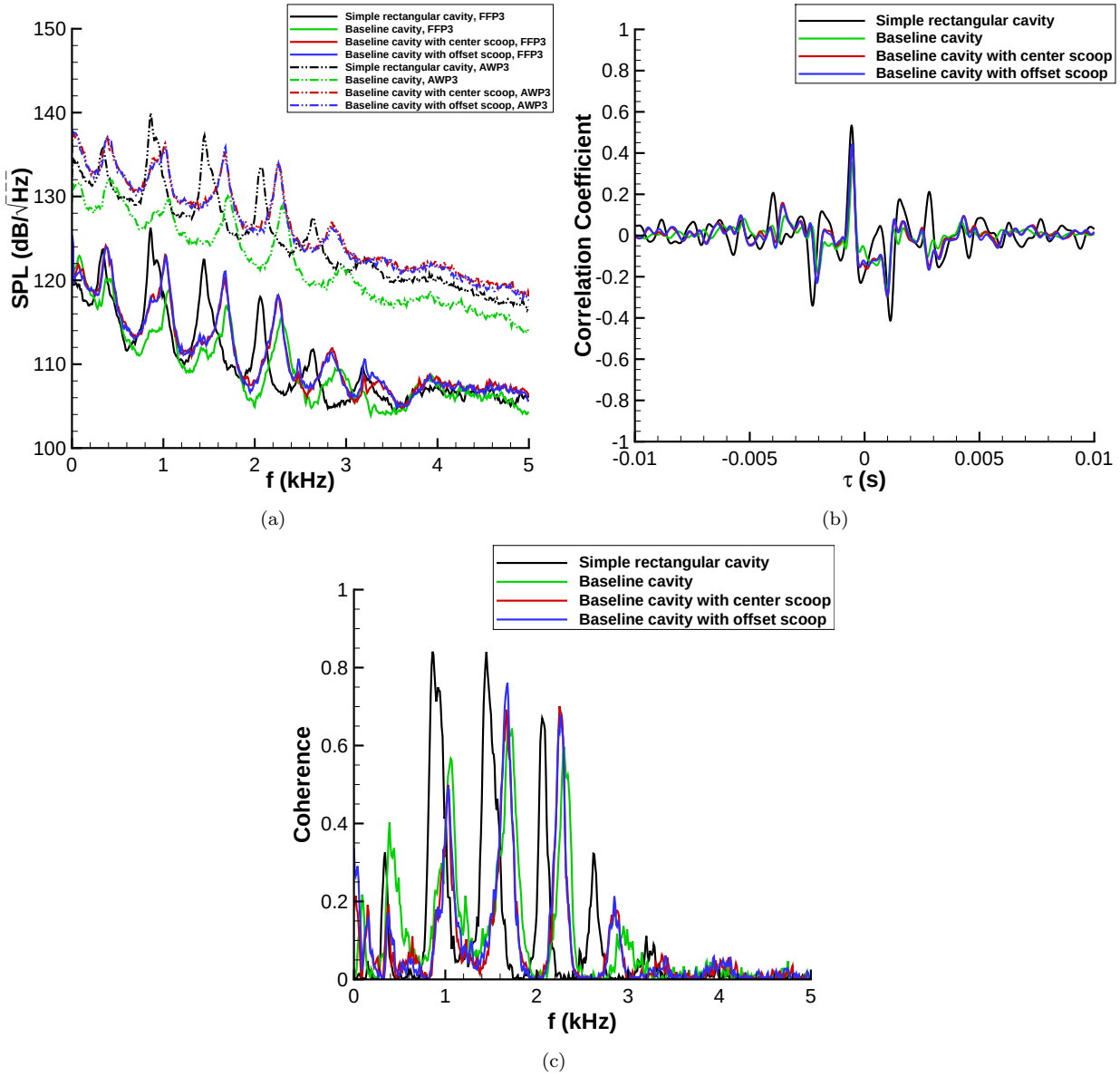

Figure 9. Effect of leading edge geometry at Mach 0.8 (a) Power-spectral density; (b) Fore-aft cross correlation; (b) Aft coherence.

cavity beneath the tooth ($\frac{a}{2H} = \frac{\sqrt{\gamma RT_0}}{2H} \approx 8$ kHz). At the opposite side of the cavity (FFP5, Fig. 10(b)), the 8.25 kHz peak is still present for the center scoop and tooth case, but it disappears with the offset scoop and tooth because there is only a small overhang above FFP5 for that configuration. Another notable change with these configurations is the dramatic increase in the second-mode amplitude for the central scoop and tooth configuration. The reason for this significant enhancement is unclear and need to be explored further as it represents a concern for structural loading of stores within a complex bay.

On the front centerline (FFP3, Fig. 10(c)), high-frequency content from the tooth is again observed near 9 kHz, and there is also an additional high-frequency peak near 7 kHz. Further downstream however (AWP3, Fig. 10(c)), the high-frequency content introduced by the tooth is no longer evident. Instead, the tooth tends to reduce the amplitude of both the modes and broadband frequencies downstream. This reduction could result from the tooth disrupting the spanwise coherence of the shear layer which has been shown to reduce cavity fluctuations.[15,16] The streamwise vorticity generated by the tooth also takes some distance to grow, so it would be expected to have less effect on the shear layer upstream and more effect downstream. These results are again qualitatively similar to Mach 1.5,[25] though the ≈ 8 kHz peak generated by the front overhang is less apparent because of the much higher frequency Rossiter modes present in the supersonic spectra.

III.E. Effect of changing L/W: side insert

Varying internal geometry can also affect the cavity pressure fluctuations. Fig. 11(a) shows PSD's in the complex geometry at FFP5, with and without the side insert. The insert has a significant effect on the cavity flow. The second and fourth Rossiter modes are enhanced, and higher frequency modes appear in the spectra. At the same time, the amplitude of the first and third Rossiter modes is decreased. This effect is seen throughout the cavity, primarily at the upstream end and in front of the insert. The side insert also results in much higher broadband fluctuations than are observed without the side insert (Fig. 11(b)). This influence decreases somewhat along the centerline and further downstream, though the higher frequencies still remain elevated even on the aft cavity wall.

The amplification of some Rossiter modes while other modes are decreased can be explained by considering the Rossiter modes of a shorter cavity with a length of L/2 (L - side insert length). The Rossiter modes of the full and half length cavities are shown in red and blue, respectively. The frequencies of the second and fourth Rossiter modes of the full-length cavity are near mode frequencies of the shorter cavity, which explains why they are enhanced. Also, the higher frequencies that are seen in the spectra with the side insert, correspond to higher frequency Rossiter modes of the shorter cavity. Because the baseline cavity with side insert is a combination of cavity lengths, the spectra appear to incorporate Rossiter mode frequencies from both cavities.

Other configurations with the side insert showed similar enhancements of the second and fourth Rossiter modes and broadband fluctuations, especially in front of the side insert and at the upstream end of the cavity. The first and third modes typically stayed the same amplitude, or decreased somewhat in amplitude.

III.F. Effect of doors

The presence of doors in the complex geometry has a dramatic effect on the measured pressure spectra, more than any other configurational change. The results for two open doors and for one open and closed door are shown in Fig. 12. At the front of the cavity (Figs. 12(a) and 12(b)), the presence of two open doors are seen to enhance both the Rossiter mode amplitudes as well as broadband frequency components in the spectra. The peak frequency of the modes is also seen to shift higher, in agreement with other door studies.[19] When one door is closed, Rossiter modes are further enhanced and additional high-frequency content is generated, particularly underneath the closed door (FFP1, Fig. 12(a)). The approximately 8 kHz peak that is observed under the leading edge tooth overhang is also enhanced with the closed door, but shifts to a slightly higher frequency of 8.5 kHz. At the open end of the cavity (FFP5, Fig. 12(b)), additional peaks and resonances are still observed and have higher amplitudes than even the two open door configuration.

Fig. 13(a) shows the coherence between sensors FFP2 and FFP4 at the front of the cavity for both door configurations. The two door open case has high coherence levels for the lowest modes. The coherence then drops to zero for higher frequency content that is mostly broadband in the PSD's. The one door closed case, however, has high coherence levels extending to higher resonant frequencies. These high coherence levels correspond to the high-amplitude resonant frequencies observed in the PSD's.

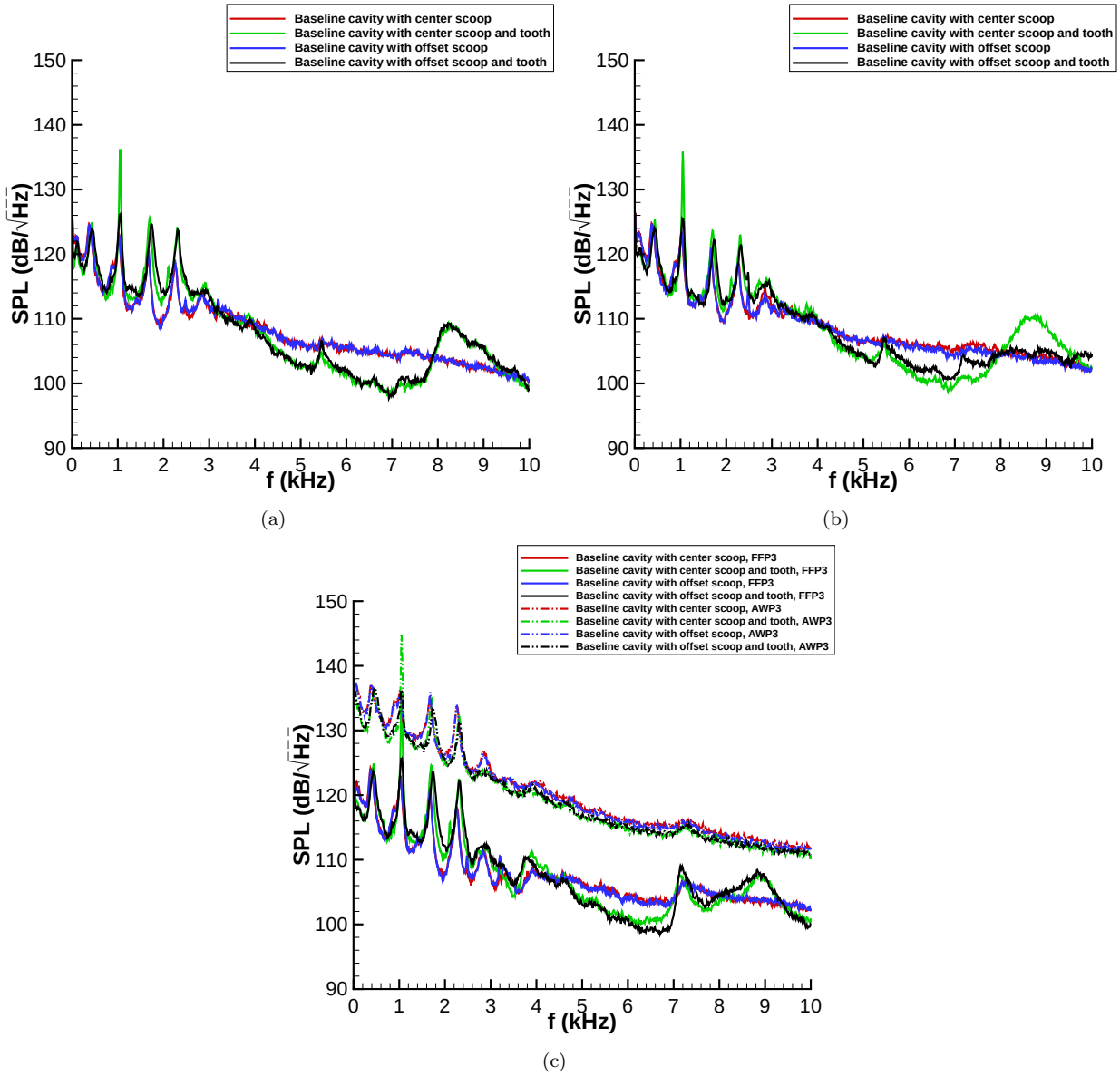

Figure 10. Effect of leading edge tooth on power spectral densities at Mach 0.8 (a) FFP1; (b) FFP5; (d) FFP3 and AWP3.

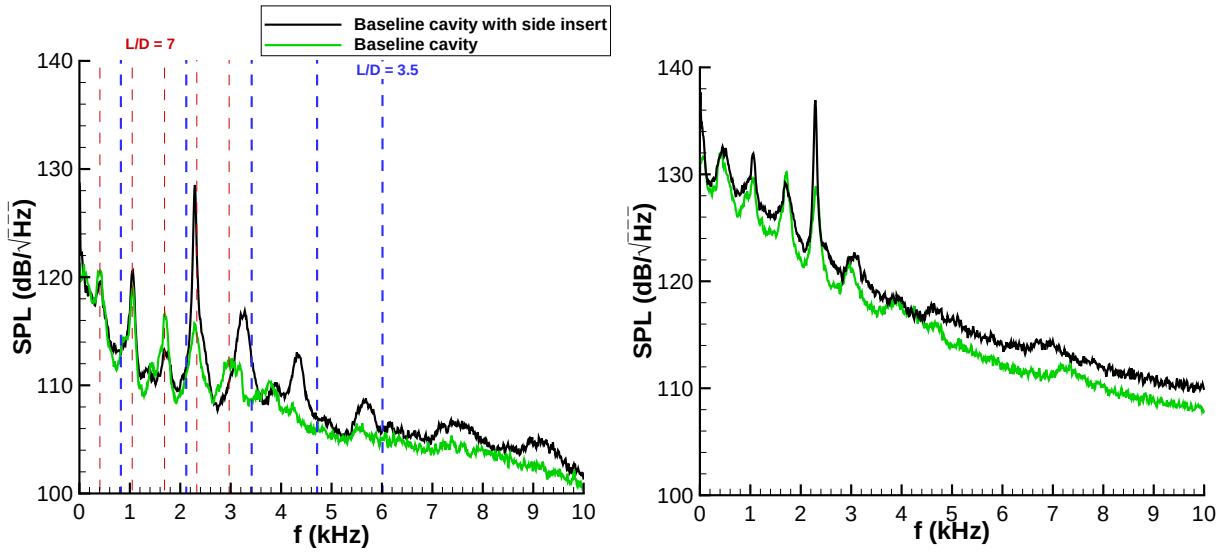

(a)

Figure 11. Effect of side insert on power-spectral densities at Mach 0.8 (a) FFP5; (b) AWP3.

At the aft end of the cavity (Figs. 12(c) and 12(d)), the broadband fluctuations of the two open door case gradually take over as the 'worst case' configuration. High frequency resonances are still generated underneath the closed door (AWP1, Fig. 12(c)); however, they are lower in amplitude than the corresponding broadband levels in the two open door configuration. At the open end of the cavity (AWP5, Fig. 12(d)), the fluctuations approach the level of the two open door configuration. Coherence levels across the cavity width tell a similar story (Fig. 13(b)) to the pressure spectra. Aft coherence levels have dropped in comparison to the cavity front. However, the coherence levels remain highest for the resonant frequencies observed in the PSD's. As a result, the one open door case has much higher coherence levels than the two open door case.

III.G. Effect of ramped floor

Another internal geometry parameter that was tested was a ramped cavity floor. This ramp decreases the cavity depth at the front, and gradually deepens to the same depth as the flat floor at the rear. Fig. 14 shows the effect of the ramp at the front, center, and rear of the cavity for two complex configurations. Most configurations show only a minor effect of the ramp, similar to Fig. 14(a). The ramp tends to decrease the mode amplitudes slightly and sometimes alters the broadband frequency amplitudes, though the effect is usually limited. However, in the case of one open and closed door, the ramp has a dramatic effect on the spectra. This is particularity true with the presence of the side insert (Fig. 14(b)). The broadband fluctuations and mode amplitudes are much higher with the ramped floor configuration throughout the cavity. This effect may be because the ramped floor decreases the area under the closed door, leading to higher frequency content that then resonates throughout the cavity. This effect is exaggerated by the presence of the side insert, which also amplifies higher frequency components as described previously. This case demonstrates the complex interaction that can occur between different cavity components, resulting in much higher loadings than a simple geometry.

The overall effect of the complex geometry can be seen by comparing measurements in the simple rectangular cavity to these complex configurations (Fig. 15). Much higher frequency content extending to 8 kHz is found with the presence of the complex geometry, while the rectangular cavity modes are limited to below 4 kHz. Also, the Rossiter modes of the complex configuration are usually shifted in frequency and have much higher amplitudes than the simple rectangular cavity. Broadband frequency components measured at the aft wall of the cavities are also significantly higher in the complex configurations. These changes show the need to consider the complex geometric changes and their effect on the resulting loading of aircraft bays when designing for flight.

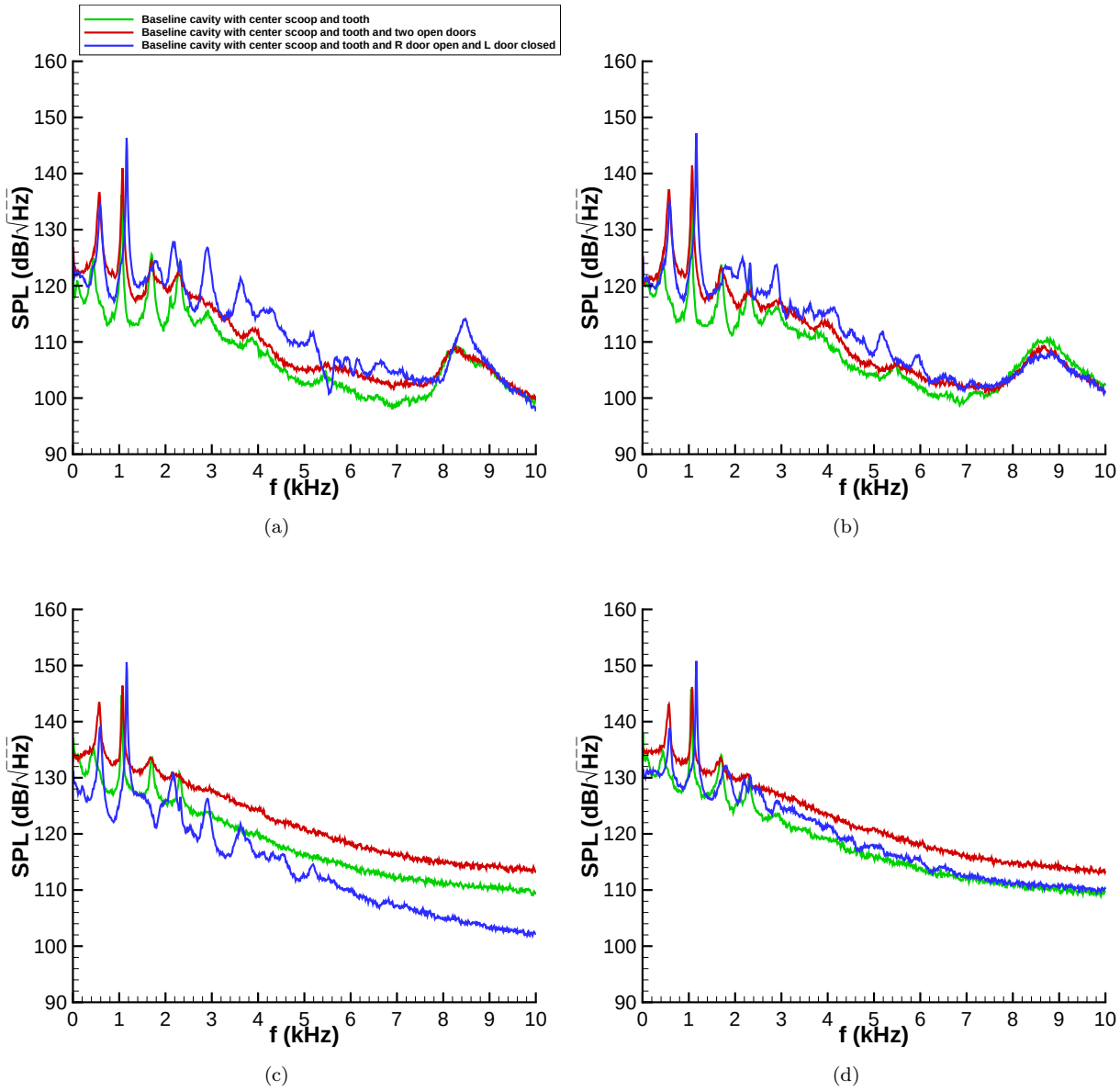

Figure 12. Effect of doors on cavity power-spectral densities at Mach 0.8 (a) FFP1; (b) FFP5; (c) AWP1; (d) AWP5.

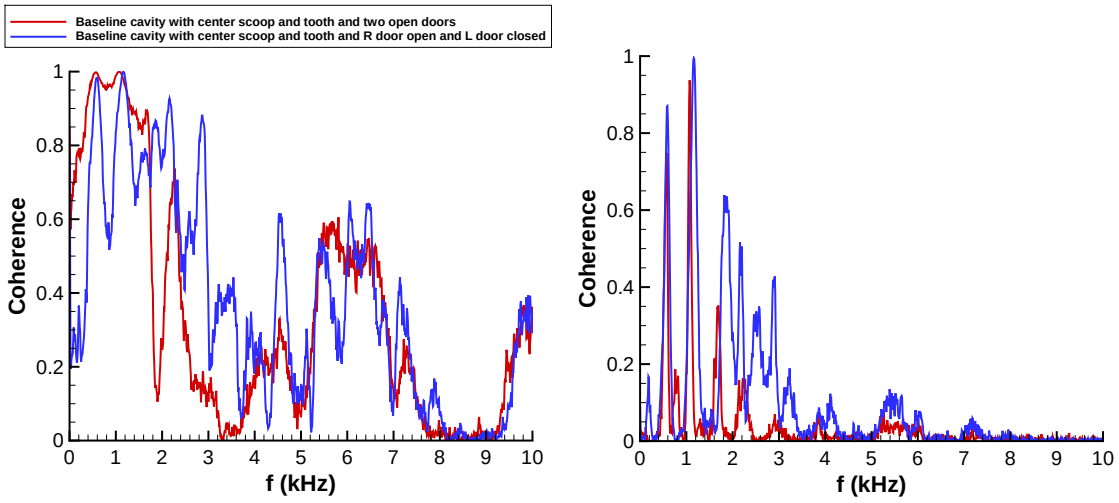

(a) (b)

Figure 13. Effect of doors on coherence at Mach 0.8 (a) Front (FFP2–FFP4); (b) Aft (AWP2–AWP4).

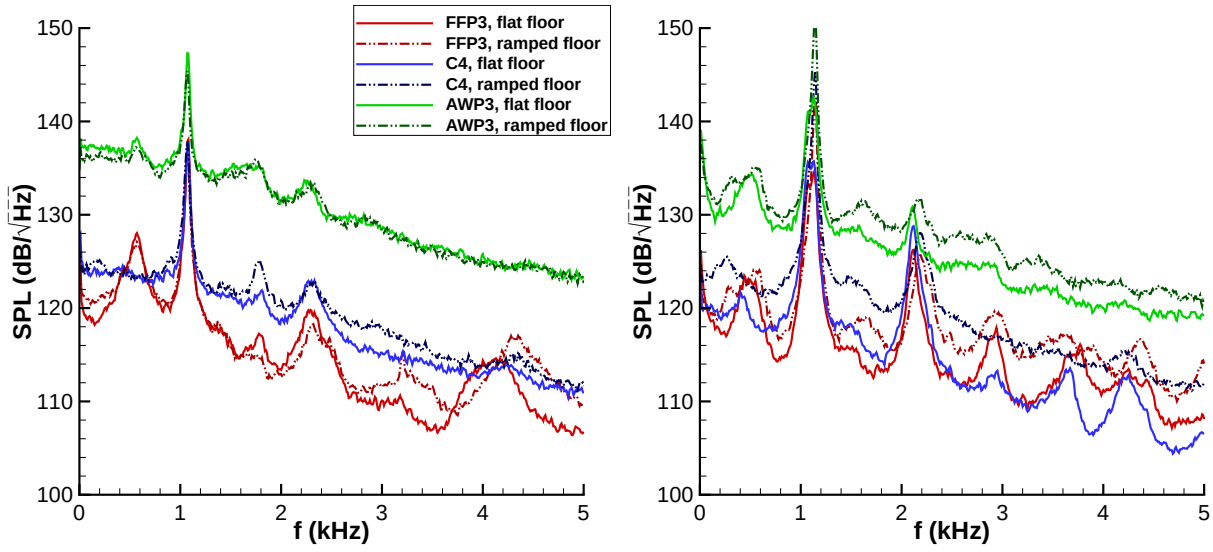

(a) (b)

Figure 14. Effect of ramped floor on cavity power-spectral densities at Mach 0.8 (a) Baseline cavity with center scoop and tooth and two open doors and side insert; (b)Baseline cavity with center scoop and tooth and R door open and L door closed and side insert.

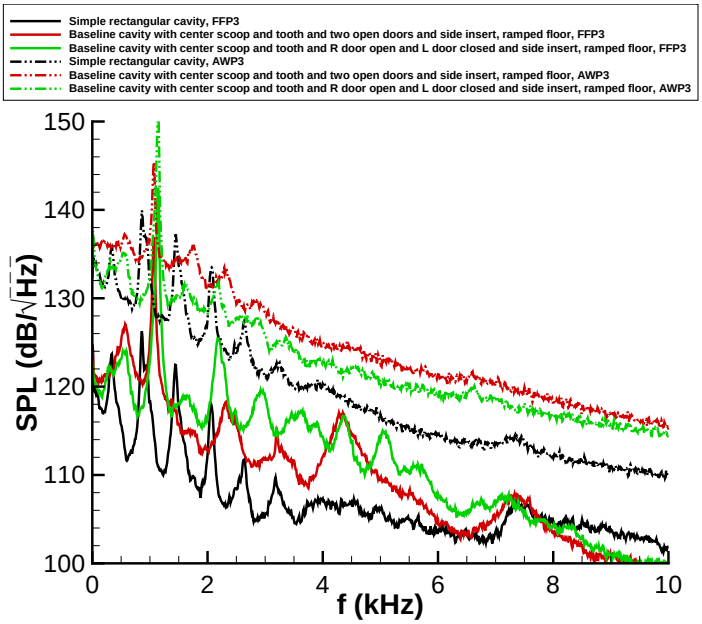

Figure 15. Combined effect of complex geometry on cavity power-spectral densities at Mach 0.8.

III.H. Mach number effects

A comparison can be made between similar configurations in both subsonic and supersonic flow. The most complex configuration tested at both subsonic and supersonic Mach numbers was the baseline cavity with the center scoop and tooth and side insert. Unfortunately, doors could not be tested in supersonic flow because of the additional tunnel blockage they created. Fig. 16 shows a comparison between Mach 0.8 and Mach 1.5. Mach 0.8 results were typical of subsonic testing between Mach 0.6–0.9 while Mach 1.5 results were typical of supersonic cases including Mach 2 and 2.5. At the front of the cavity (FFP5), the effect of the complex geometry is clearly seen at both Mach numbers. The complex features add additional high frequencies in the spectra and the Rossiter modes shift upwards in both cases. The effect of the front overhang shows up more clearly at Mach 0.8 as a strong peak above 8 kHz. At Mach 1.5, the effect is not as clear because of the presence of many additional high frequencies in the spectra. At both Mach numbers, the second and fourth Rossiter modes are enhanced, while the first and third modes remain the same or are decreased. This response to the side insert corresponds to the cavity acting as a dual-length cavity as discussed in Section III.E. The presence of these amplified peaks has significant implications for store response at both Mach numbers.

Further downstream at AWP3, there are larger differences between the two Mach numbers. The complex features at Mach 1.5 are actually suppressing all the modes downstream, while at Mach 0.8, there is once again an enhancement of some modes and a decrease in other modes. Also, the broadband fluctuations on the aft wall are generally higher at Mach 0.8 while they approach the same level at Mach 1.5. These comparisons are typical of subsonic to supersonic comparisons for other complex configurations. Geometric changes such as the front tooth and the presence of the side insert tended to have a stronger effect in subsonic flow compared to supersonic flow.

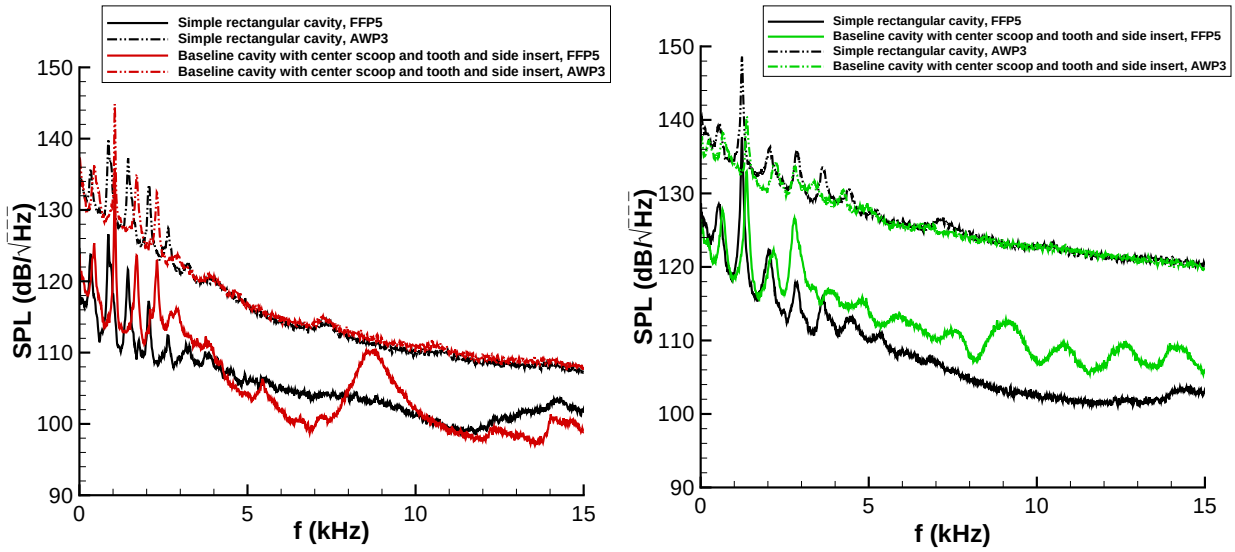

Figure 16. Comparison of complex geometries at Mach 0.8 and 1.5.

IV. Concluding Remarks

A complex cavity has been designed to allow representative features of an aircraft bay to be incorporated into a basic rectangular cavity. This allows the effect of varying inlet geometries, internal cavity variations, and doors on the cavity flow to be isolated and studied. Some changes had only minor effects. For example, the spanwise location of the leading edge inlet geometry had little change on the resulting spectra. The presence of a ramped floor geometry also tended to have only a minor effect on the measured pressure spectra in simpler configurations.

Other configurational changes had a much larger effect. The presence of a leading edge scoop which varied the height of the shear layer with respect to the aft cavity wall had a large effect on the amplitude of broadband fluctuations at the aft wall. Also, configurations that constricted the flow led to large changes in the measured pressure spectra. A leading edge tooth that created an overhang at the front of the cavity led to higher frequency resonances in the flow at the front of the cavity. Downstream, however, the effect was minor. A side insert placed in the cavity acted like a hybrid dual-length cavity and created Rossiter modes corresponding to both a long and short cavity. This lead to much higher frequency content in the spectra, particularly at the front of the cavity and in front of the side insert. The presence of doors also led to a dramatic change in the spectra and provided the worst loading for all cases tested. One open and closed door created resonant fluctuations that dominated the spectra at the front of the cavity. These were strongest under the closed door, but resonated across the span. Further downstream, the two open doors led to the highest broadband frequency content measured on the aft cavity wall.

The complex variations created much higher frequency content in the measured pressure spectra in comparison to a simple rectangular cavity. The amplitude of a specific mode seemed to be more prone to enhancement by the presence of complex features. Also, in some cases where the flow was constricted, parametric changes that had little effect in other combinations interacted with the restricting complex features to generate much higher loading conditions. For example, the ramped floor which typically had little effect for simpler combinations, led to much high mode amplitudes and broadband fluctuations when tested with a closed door and side insert. These changes highlight the need to consider complex effects when defining loading environments for aircraft bays.

Acknowledgments

The authors thank Srinivasan Arunajatesan and Matthew Barone for helpful discussions on cavity dynamics. Tom Grasser designed and oversaw construction of the complex geometry hardware.

References

[1]Rockwell, D. and Naudascher, E., "Review-Self-Sustaining Oscillations of Flow Past Cavities," *Journal of Fluids Engineering*, Vol. 100, No. 2, 1978, pp. 152–165.

[2]Rowley, C. W. and Williams, D. R., "Dynamics and Control of High-Reynolds-Number Flow over Open Cavities," *Annual Review of Fluid Mechanics*, Vol. 38, 2006, pp. 251–276.

[3]Rossiter, J. E., "Wind-Tunnel Experiments on the Flow over Rectangular Cavities at Subsonic and Transonic Speeds," Reports & Memoranda 3438, Aeronautical Research Council, October 1964.

[4]Tracy, M. B. and Plentovich, E. B., "Cavity Unsteady-Pressure Measurements at Subsonic and Transonic Speeds," NASA Technical Paper 3669, December 1997.

[5]Dix, R. E. and Bauer, R. C., "Experimental and Theoretical Study of Cavity Acoustics," Tech. Rep. AEDC-TR-99-4, Arnold Engineering Development Center, May 2000.

[6]Heller, H. H. and Bliss, D. B., "The Physical Mechanism for Flow-Induced Pressure Fluctuations in Cavities and Concepts for their Suppression," AIAA Paper 75-491, March 1975.

[7]Wagner, J. L., Beresh, S. J., Casper, K. M., Henfling, J. F., Spillers, R. W., Hunter, P. S., Blecke, J. C., and Mayes, R. L., "Simultaneous Vibration and Acoustic Measurements of a Store in Compressible Open Cavity Flow," AIAA Paper 2013-0228, January 2013.

[8]Beresh, S. J., Wagner, J. L., Pruett, B. O. M., Henfling, J. F., and Spillers, R. W., "Supersonic Flow over a Finite-Width Rectangular Cavity," *AIAA Journal*, 2014, AIAA Early Edition.

[9]Kannepalli, C., Chartrand, C., Birkbeck, R., Sinha, N., and Murray, N., "Computational Modeling of Geometrically Complex Weapons Bays," AIAA Paper 2011-2774, June 2011.

[10]Plentovich, E., Chu, J., and Tracy, M. B., "Effects of Yaw Angle and Reynolds Number on Rectangular-Box Cavities at Subsonic and Transonic Speeds," Tech. Rep. NASA TP-3099, 1991.

[11]Disimile, P. J., Toy, N., and Savory, E., "Pressure Oscillations in a Subsonic Cavity at Yaw," *AIAA Journal*, Vol. 36, No. 7, July 1998, pp. 1141–1148.

[12]Lee, B. H. K., Orchard, D. M., and Tang, F. C., "Flow Past a Yawed Rectangular Cavity in Transonic and Low Supersonic Flows," *Journal of Aircraft*, Vol. 46, No. 5, September – October 2009, pp. 1577–1583.

[13]Tracy, M. B., Plentovich, E. B., Hemsch, M. J., and Wilcox, F. J., "Effect of Sweep on Cavity Flow Fields at Subsonic and Transonic Speeds," Tech. Rep. NASA TM 2012-217577, NASA Langley Research Center, May 2012.

[14]Cattafesta, L., Williams, D. R., Rowley, C. W., and Alvi, F., "Review of Active Control of Flow-Induced Cavity Resonance," AIAA Paper 2003-3567, June 2003.

[15]Ukeiley, L., Sheehan, M., Coiffet, F., Alvi, F., Arunajatesan, S., and Jansen, B. J., "Control of Pressure Loads in Geometrically Complex Cavities," *Journal of Aircraft*, Vol. 45, No. 3, May–June 2008, pp. 1014–1024.

[16]Arunajatesan, S., Kannepalli, C., Sinha, N., Sheehan, M., Alvi, F., Shumway, G., and Ukeiley, L., "Suppression of Cavity Loads Using Leading-Edge Blowing," *AIAA Journal*, Vol. 47, No. 5, May 2009, pp. 1132–1144.

[17]Dudley, J. G. and Ukeiley, L., "Suppression of Fluctuating Surface Pressures in a Supersonic Cavity Flow," AIAA Paper 2010-4974, June 2010.

[18]Shaw, L., Clark, R., and Talmadge, D., "F-111 Generic Weapons Bay Acoustic Environment," AIAA Paper 87-0168, January 1987.

[19]Murray, N. E. and Jansen, B. J., "Effect of Door Configuration on Cavity Flow Modulation Process," *AIAA Journal*, Vol. 50, No. 12, December 2012, pp. 2932–2937.

[20]Panickar, M. B., Murray, N. E., Jansen, B. J., Joachim, M. P., Birkbeck, R., Kannepalli, C., and Sinha, N., "Reduction of Noise Generated by a Half-Open Weapons Bay," *Journal of Aircraft*, Vol. 50, No. 3, May–June 2013, pp. 716–724.

[21]Stallings, R. L., Plentovich, E., Tracy, M. B., and Hemsch, M. J., "Measurements of Store Forces and Moments and Cavity Pressure for a Generic Store In and Near a Box Cavity at Subsonic and Transonic Speeds," Tech. Rep. NASA TM-4611, May 1995.

[22]Lee, B. H. K., "Effect of Cavity Store on Internal Weapons Bay Floor Pressure Distributions," *Journal of Aircraft*, Vol. 47, No. 2, March–April 2010, pp. 732–735.

[23]Wagner, J. L., Casper, K. M., Beresh, S. J., Hunter, P. S., Spillers, R. W., Henfling, J. F., and Mayes, R. L., "Experimental Investigation of Fluid-Structure Interactions in Compressible Cavity Flows," AIAA Paper 2013-3172, June 2013.

[24]Bartel, H. W. and McAvoy, J. M., "Cavity Oscillation in Cruise Missile Carrier Aircraft," Tech. Rep. AFWAL-TR-81-3036, Air Force Wright Aeronautical Laboratories, June 1981.

[25]Casper, K. M., Wagner, J. L., Beresh, S. J., Henfling, J. F., Spillers, R. W., and Pruett, B. O. M., "Complex Geometry Effects on Supersonic Cavity Flows," AIAA Paper 2014-3025, June 2014.

[26]Wagner, J. L., Casper, K. M., Beresh, S. J., Henfling, J. F., Spillers, R. W., and Pruett, B. O. M., "Mitigation of Wind Tunnel Wall Interactions in Subsonic Cavity Flows," AIAA Paper 2014-3026, June 2014, also submitted to Experiments in Fluids.

[27]Korkegi, R. H., "Comparison of Shock-Induced Two- and Three-Dimensional Incipient Turbulent Separation," *AIAA Journal*, Vol. 13, No. 4, 1975, pp. 534–535.

[28]Collins, F. G., Wu, J. M., and Moulden, T. H., "Examination of Turbulent Transonic Flow Over Ramp-Compression-Corners," AIAA Paper 78-1166, July 1978.

[29]Zhuang, N., Alvi, F., Alkislar, M. B., and Shih, C., "Supersonic Cavity Flows and Their Control," *AIAA Journal*, Vol. 44, No. 9, September 2006, pp. 2118–2128.